KINETICS OF EUTECTOID TRANSFORMATION IN A Cu - 20.15 at. % In ALLOY

by

MAHESH KUMAR BHATIA

DEPARTMENT OF METALLURGICAL ENGINEERING

INDIAN INSTITUTE OF TECHNOLOGY KANPUR

MAY, 1991

KINETICS OF EUTECTOID TRANSFORMATION IN A Cu - 20.15 at. % In ALLOY

A Thesis Submitted
in Partial Fulfilment of the Requirements
for the Degree of
MASTER OF TECHNOLOGY

by

MAHESH KUMAR BHATIA

to the

DEPARTMENT OF METALLURGICAL ENGINEERING
INDIAN INSTITUTE OF TECHNOLOGY KANPUR

MAY, 1991

CERTIFICATE

This is to certify that the matter embodied in the thesis entitled "Kinetics of Eutectoid Transformation in A Cu - 20.15 at. % In Alloy" by Mr. Mahesh Kumar Bhatia for the award of Degree of Master of Technology of the Indian Institute of Technology, Kanpur is a record of bona-fide research work carried out by him under my supervision and guidance. The results embodied in this thesis have not been submitted elsewhere for the award of any degree and diploma.

Dr. S. P. Gupta
Professor
Department of Metallurgical Engineering
Indian Institute of Technology
Kanpur.

May, 1991

ACKNOWLEDGEMENTS

I am deeply indebted to Dr. S.P. Gupta for his invaluable guidance and encouragement throughout the course of this work.

I am thankful to Mr. K.P. Mukherjee and Mr. P.K. Paul for the help rendered by them in the laboratory work.

Finally, I appreciate the excellent job done by Mr. R.N. Srivastava for typing the manuscript and all others who helped at many steps.

M.K. BHATIA

CONTENTS

LIST OF TABLES

LIST OF FIGURES

ABSTRACT

The growth kinetics of the product of the eutectoid transformation has been studied in a Cu - 20.15 at. pct. In alloy in the temperature range 570 to 710 K. The Cu-In alloy was observed to undergo the eutectoid transformation into a lamellar structure consisting of alternate lamellae of α and δ phases. Pearlite was also observed to form into a granular morphology. Lattice parameter measurements indicated that the α phase has the composition corresponding to the equilibrium solvus. Analysis of the growth kinetics has indicated that the eutectoid transformation in this system is controlled by interface diffusion of solute at the α/β interface.

CHAPTER - I

INTRODUCTION

Pearlite of Fe-C system is one of the most extensively studied structure. It got its importance due to its strong influence on hardenability, and due to its being one of the most important solid-state transformations.

The austenite in Fe-C system can result into two different products, bainite and pearlite, both consist of the same constituents - ferrite and cementite. In pearlite the two product phases, arrange themselves as alternate lamellae. Now any eutectoid transformation product having alternate lamellae - no matter what the system is - is called pearlitic structure.

A number of attempts have been made in the past to resolve whether α or β phase of the pearlite acts as nucleus for the formation of pearlite. In steels it was known by then that nuclei for bainite are crystals of Widmanstatten ferrite, it was assumed that the nucleus of pearlite was platelet of cementite of a Widmanstatten relation with parent austenite. Benedicks [1] long before had suggested that proeutectoid ferrite as well as cementite would act as 'germs' for the formation of fine pearlite. It was confirmed that in hypereutectoid steels cementite will normally form first and will then nucleate pearlite; in hypoeutectoid steels ferrite will form first and then nucleate pearlite.

The fine lamellar pearlite structure which forms, as explained above, has been found in many non-ferrous systems as well. In the broad sense, the term pearlite reaction is defined as those reactions in which two low temperature phases precipitate co-operatively and essentially simultaneously from the product phase in a manner which results into no overall change in composition of either of the parent phase or two phase product as the reaction interface moves at constant velocity. The primary characteristic of the pearlite reaction, is the steady state nature of the reaction kinetics rather than the morphology of the reaction products. Lamellar structure is one of the many possible morphologies.

In Chapters to follow the theory has been treated for eutectoid reaction $\gamma \rightarrow \alpha + \beta$, though the actual reaction in Cu-In system studied is $\beta \rightarrow \alpha + \delta$.

1.1 FORMATION OF PEARLITE

1.1.1 The Orientation Relationship

Developed for steels the Smith theory [2] suggested that a crystal of proeutectoid ferrite formed at the grain boundary between two austenite grains has some definite orientation relationship with one of the grains and can make semicoherent interface with this austenite grain. But with neighbouring grain the ferrite cannot form any particular orientation relationship and thus forms incoherent interface. Since an incoherent interface consumes less

energy at small undercooling the incoherent interface moves. With higher undercooling the free energy available is more and thus the semicoherent interface can also move.

To prove this hypothesis, a sample was transformed just above the eutectoid temperature so that proeutectoid ferrite could form along austenite grain boundaries. Upon further transformation at subcritical temperature where both pearlite and bainite could form, it was found that pearlite forms along ferrite-austenite boundary in one grain while in neighbouring grain bainite was observed, Figure 1.

On the basis of Smith's hypothesis [2], many possible morphologies of ferrite depending upon the nature of interfaces have been suggested, Figure 2. In these figures straight lines show semicoherent interface. The semicoherent interface may sometimes form in both the neighbouring grain which shows that semicoherent interface can form even when there is deviation from ideality in orientation relationship. The interface however, then differs in the degree of coherency in the two grains. For this the Smith's hypothesis [2] can be related with the growth rates of pearlite in two ways:

(a) The mobility of incoherent interfaces being more.

(b) The diffusivity may appreciably increase along an incoherent boundary allowing a rapid lateral diffusion and resulting in high growth rates.

A microscopic study has indicated that morphologies formed are the same in both hyper- and hypo-eutectoid

compositions. This then suggests that for pearlite growth co-operation between both phases α and β is of importance. This can further be appreciated when it was found that twin boundaries have similar effects on pearlite growth as two parent phase's grains of different orientations.

1.1.2 Nucleation and Growth of Pearlite

There are two mechanisms for growth of pearlite. These are

(a) Edge-wise growth

(b) Side-wise growth.

In case of edge-wise growth the interface between the pearlite and parent phase moves in the direction perpendicular to itself. In side-wise growth on the other hand, new lamellae of either phase (α or β) nucleates and grows along interface of the existing lamellae with matrix. But such type of growth has never been found. A steel sample was partially transformed at close to eutectoid temperature. Then it was brought to lower temperature. Had side-wise growth been possible the new lamellae would have been grown with new interlamellar spacing in the region of existing coarse pearlite as well. But the case was never found. Instead the interlamellar spacing corresponding to new temperature was obtained by branching of the already grown coarse pearlite at both the three phase contact point of lamellae.

In case of edge-wise growth considering solute diffusion, e.g. carbon in steels, as the transformation

controlling reaction calculations were done. Initially diffusion from the tips of cementite lamellae was considered. This type of diffusion called volume diffusion, produced growth rates less than practically observed. The idea of diffusion along pearlite-matrix interface came forward which however, needs better understanding of the interface between pearlite and parent phase.

Attempts were made by Darken and Fiscner [3] to understand the nature of interface between pearlite-austenite in a number of carbon and low alloy steels. The most distinctive feature of the microstructure was the observation of ferrite gap between cementite lamellae and austenite matrix. The calculations were then made by taking ferrite gap as the distance a carbon atom covers to join cementite platelet. The model, however, has been refuted by Hillert [4] who proposed that the ferrite gap between cementite and austenite occurs during quenching of the sample from transformation temperature.

On the basis of microstructural observation of austenite to pearlite transformation the following sequence can be considered in hypereutectoid steels:

(a) Cementite nucleates at the grain boundary forming a network thus displacing the austenite composition towards the hypoeutectoid side in the Fe-C diagram, Figure 3.

(b) Ferrite which nucleates at the cementite-austenite interface grows along the interface isolating cementite from the remaining austenite.

(c) When growing along cementite-austenite interface, the ferrite may reach a hole or a sharp edge of the cementite. There the ferrite may not be able to isolate the cementite completely from austenite. An arm of cementite grows out from the network and remains in contact with the austenite.

(d) Due to growth of ferrite the austenite composition moves towards hypereutectoid side favouring growth of cementite arm. The cementite then grows.

(e) During further growth branching occurs till the spacing is close to the value characterized by the temperature.

Since the nature of the product formed is same in majority of the alloys studied, it has been established that the transformation takes place similar to that stated for steels above.

The above mentioned mechanism further proves that a pearlite unit is composed of two interwoven crystals one of ferrite and the other of cementite.

Many factors affect the growth of a pearlite colony such as:

A) Effect of Grain Boundaries: As already mentioned, the pearlite colony which forms at the grain boundary of parent phase grows only in one of the adjacent grains. Likewise the growing pearlite colony rarely finds next grain of parent phase giving rise to coherency. Hillert [4] has

found that grain boundaries usually have no effect on the growth of a pearlite colony though the direction of lamellae may change due to effect of high energy grain boundary on the steady state conditions at pearlite front.

However, if a pearlite front strikes a grain boundary at low angle the chances that co-operation between the two precipitating phases is lost, becomes more.

B) **Effect of Twin Boundaries:** The presence of twins in large number increases the chances of forming coherent interface between parent and product phases. Thus a growing pearlite colony may form Widmanstatten structure or a Widmanstatten may alter into normal pearlite as the orientation changes on the other side of the twin boundary. The effect of twin boundaries have been found to increase with decreasing transformation temperature, due to twin boundaries acting as nucleation sites at such temperatures.

1.2 KINETICS OF PEARLITE REACTION

The study of growth of pearlite into austenite has been started since many years back, theoretically as well as experimentally. It is evident from studies carried out that this mode of eutectoid decomposition is common to many non-ferrous alloy systems as well, for example in Cu-In, Cu-Al, Al-Zn, Al-Cu etc.

The earliest theoretical contributions were made by Brandt [5], Scheil [6], Zener [7], and Hillert [8]. It was assumed initially that the growth of isothermal pearlite

was a volume-diffusion controlled reaction, the solute diffusion occurring in the matrix ahead of the interface, keeping local equilibrium. Since the average composition of the product (α and β) is same as that of matrix (γ) far ahead of the advancing interface, it was assumed that growth rate must be constant.

It was found, however, that theories based on volume diffusion of solute along advancing interface give growth rates much less than experimentally observed. Boundary diffusion controlled theories were then developed which were derived from earlier treatments of discontinuous precipitation by Turnbull [9] and Cahn [10].

1.2.1 Zener's Treatment

Hillert [8] described Zener's treatment [7] of the eutectoid transformation pointing out that Zener was the first one to take surface effects into consideration. The theoretical treatment of eutectoid transformation includes effect of surface energies involved in transformation. The driving force available for the reaction is consumed for diffusion of solute and surface energies of surfaces formed between α and β phases of the lamellar structure. The interfacial energy associated with the interface is

$$\Delta G_m^s = \frac{2\gamma V_m}{S} \qquad (1)$$

where

γ = Specific surface energy

V_m = Molar volume

S = Interlamellar spacing (sum of thickness of α and β lamellae).

If we assume that low solute containing phase α forms first, the solute concentration in γ near α-γ interface increases and the concentration profile at the interface will have shape as shown in Figure 4 schematically. For the growth of ferrite the concentration of the solute must diffuse in the γ away from the interface. The ferrite grows as fast as diffusion permits. The concentration profile of solute near β/γ interface (Figure 5) shows that the γ phase must provide solute which must move down the concentration gradient and join the β-phase. The growth is again limited by diffusion of solute through the γ matrix. The composition profiles at α/γ and β/γ interfaces are complementry because one requires that excess solute diffuse into the neighbouring matrix whereas the other requires solute for continued growth. Thus instead of solute transfer occurring separately into the volume of parent phase, the solute transfer may occur from the edges of the growing α-phase to the edges of the growing β-phase. Such diffusion will produce co-operative growth of α- and β-phases.

The solute concentration at γ/α and γ/β interfaces can also be illustrated with the help of the free energy composition diagram of α, β and γ phases shown schematically in Figure 6. When the α/β phases of very large spacing are considered the composition at the β/γ interface

comes out to be ${}^{e}X_B^{\beta/\gamma}$ and at α/γ comes out to be ${}^{e}X_B^{\alpha/\gamma}$. The concentration gradient $\Delta X_B^e (= {}^{e}X_B^{\alpha/\gamma} - {}^{e}X_B^{\beta/\gamma})$ causes diffusion to occur from one type of interface to the other. But when the interlamellar spacing is not very large the free energy curves of the α and β are shifted upward as given by Gibbs-Thomson relation for spacing S

$$\Delta^{s}G_m^{\alpha} = \Delta^{\infty}G_m^{\alpha} + \frac{2\gamma V_m}{S} \qquad (2)$$

Following the same method of constructing common tangent at α and β phases free energy curves at new position, the concentration gradient $\Delta X_B (= {}^{s}X_B^{\alpha/\gamma} - {}^{s}X_B^{\beta/\gamma})$ comes out to be less than ΔX_B^e. If the interlamellar spacing S is decreased further a situation will come when ΔX_B equals zero. At such situation there will not be any diffusion of solute and growth will not occur. At this instant, the interlamellar spacing called critical spacing by Zener [7], the free energy available for growth of pearlite would have to go to interfaces. Thus at critical spacing S_c

$$\Delta G_m^T = \frac{2\gamma V_m}{S_c} \qquad (3)$$

The free energy left to drive the diffusion is thus decreased by a factor

$$\frac{\Delta G_m^T - \Delta G_m^S}{\Delta G_m^T} = \left[\frac{2\gamma V_m}{S_c} - \frac{2\gamma V_m}{S}\right] / \left[\frac{2\gamma V_m}{S_c}\right] = \left[1 - \frac{S_c}{S}\right]$$

Zener [7] realised that total free energy available to drive the eutectoid reaction is proportional to, ΔX_B^e

and that for diffusion to occur is proportional to ΔX_B. Thus

$$\frac{\Delta X_B}{\Delta X_B^e} = \frac{\Delta G_m^T - \Delta G_m^S}{\Delta G_m^T} = \left[1 - \frac{S_c}{S}\right] \qquad (4)$$

Growth Kinetics: Let us consider the lamellar structure consisting of α and β alternate lamellae as shown in Figure 7, where

S = Interlamellar spacing

b = Aroitrary distance perpendicular to the growth direction and parallel to the planer faces of the lamellae.

Considering the growth of diffusion in y-direction, the total number of moles of the solute moving away from α lamellae in y-direction from the Fick's law

$$\frac{dm}{dt} = J_1 = \frac{A^\alpha D}{V_m} \cdot \frac{dX_B}{dy} \qquad (5)$$

where

A^α = Area through which diffusion of solute takes place = $b.S^\alpha$

$\frac{dX_B}{dy}$ = Concentration gradient of solute along the interface from edge of α lamellae to that of β.

dy = Effective diffusion distance = S^α

$$\frac{dm}{dt} = \frac{2bD\ \Delta X_B}{V_m} \qquad (6)$$

If an α phase interface with γ moves with steady state velocity v then the number of moles of solute transformed is

$$\frac{dm}{dt} = \frac{v_b S^{\alpha}}{V_m} (X_B^{\gamma} - X_B^{\alpha}) \qquad (7)$$

from Lever's rule

$$S^{\alpha}(X_B^{\gamma} - X_B^{\alpha}) = S^{\beta}(X_B^{\beta} - X_B^{\gamma}) = S(X_B^{\beta} - X_B^{\alpha}) \qquad (8)$$

upon substitution of (7) and (8) in equation (6)

$$v = \frac{2D\ \Delta X_B}{f^{\alpha} f^{\beta} S(X_B^{\beta} - X_B^{\alpha})} \qquad (9)$$

From equation (4)

$$v = \frac{2D\ \Delta X_B^{e}}{f^{\alpha} f^{\beta} S(X_B^{\beta} - X_B^{\alpha})} \left[1 - \frac{S_c}{S}\right] \qquad (10)$$

1.2.2 Hillert's Treatment

In the Zener's treatment [7] discussed above for the theoretical formulations of the volume diffusion controlled growth of pearlite, Zener [7] considered only the difference in the concentration of solute (ΔX_B) at the two interfaces but ignored the individual values $X_B^{\gamma/\alpha}$, $X_B^{\gamma/\beta}$. Secondly, he ignored the effects of the concentration change due to interface shape.

Hillert [8] introduced an additional quantity which defines the concentration at the interface. He considered that the total free energy available to drive austenite to pearlite reaction is divided into several components ΔG_1, ΔG_2, ΔG_3 etc. If ΔG_m^{α} and ΔG_m^{β} are the free energies required primarily to overcome the effect of surface tension of the curved edges of the lamellae then

$$f^{\alpha} \cdot \Delta G_m^{\alpha} = L^{\alpha} \frac{2\gamma V_m}{S}$$

$$f^{\beta} \cdot \Delta G_m^{\beta} = L^{\beta} \frac{2\gamma V_m}{S} \qquad (11)$$

$$\text{or} \quad f^{\alpha} \cdot \Delta G_m^{\alpha} + f^{\beta} \cdot \Delta G_m^{\beta} = \frac{2\gamma V_m}{S} \qquad (12)$$

where L^{α} and L^{β} represent the fraction of the surface tension of the α/β interfaces which are carried by each phase.

The values of the L^{α} and L^{β} depend upon the balance of surface tension forces $\gamma^{\alpha/\beta}$, $\gamma^{\gamma/\alpha}$ and $\gamma^{\gamma/\beta}$ at the three phase junction. Hillert [8] solved the problem by dividing that part of the free energy which goes into surface energy, into two parts, as illustrated in the free-energy composition diagram (Figure 8). Hillert [8] writes for ΔG_m^{α} and ΔG_m^{β} as follows

$$\Delta G_m^{\alpha} = \frac{RT[{}^{e}X_B^{\gamma/\alpha} - {}^{s}X_B^{\gamma/\alpha}]}{X_B^{\gamma}[1 - X_B^{\gamma}]} [X_B^{\gamma} - X_B^{\alpha}]$$

and (13)

$$\Delta G_m^{\beta} = \frac{RT[{}^{e}X_B^{\gamma/\beta} - {}^{s}X_B^{\gamma/\beta}]}{X_B^{\gamma}[1 - X_B^{\gamma}]} [X_B^{\gamma} - X_B^{\beta}]$$

From Lever's rule

$$f^{\alpha}(X_B^{\gamma} - X_B^{\alpha}) = f_{\beta}(X_B^{\beta} - X_B^{\gamma}) = f^{\alpha}f^{\beta}(X_B^{\beta} - X_{\beta}^{\alpha}) \qquad (14)$$

Upon substitution in equation (11)

$$f^{\alpha} \Delta G_m^{\alpha} = L^{\alpha} \frac{2\gamma V_m}{S} = RT({}^{e}X_B^{\gamma/\alpha} - {}^{s}X_B^{\gamma/\alpha}) f^{\alpha}(X_B^{\gamma} - X_B^{\alpha})$$

$$= RT({}^{e}X_B^{\gamma/\alpha} - {}^{s}X_B^{\gamma/\alpha}) f^{\alpha}f^{\beta} \frac{(X_B^{\beta} - X_B^{\alpha})}{} \qquad (15)$$

and similarly

$$f^{\beta}\,\Delta G_m^{\beta} = RT({}^{e}X_B^{\gamma/\beta} - {}^{s}X_B^{\gamma/\beta})\, f^{\alpha}f^{\beta}\,\frac{(X_B^{\beta} - X_B^{\alpha})}{X_B^{\gamma}(1 - X_B^{\gamma})}$$

from equations (12) and (15)

$$f^{\alpha}\Delta G_m^{\alpha} + f^{\beta}\Delta G_m^{\beta} = \frac{2\gamma V_m}{S} = \frac{f^{\alpha}f^{\beta}(X_B^{\beta} - X_B^{\alpha})}{X_B^{\gamma}(1 - X_B^{\gamma})}\, RT[{}^{e}X_B^{\gamma/\alpha} - {}^{s}X_B^{\gamma/\alpha} + {}^{s}X_B^{\gamma/\beta} - {}^{e}X_B^{\gamma/\beta}]$$

or

$$\frac{2\gamma V_m}{S} = f^{\alpha}f^{\beta}\, RT[\frac{\Delta X_B^{\beta} - \Delta X_B^{\alpha}}{X_B^{\gamma}(1 - X_B^{\gamma})}]\, \Delta X_B^{e}[1 - \frac{\Delta X_B^{s}}{\Delta X_B^{e}}]$$

$$\frac{2\gamma\ V_m}{S} = \frac{2\gamma\ V_m}{S_o}\,[1 - \frac{\Delta X_B^{s}}{\Delta X_B^{e}}] \tag{16}$$

where

$$\frac{2\gamma\ V_m}{S_o} = f^{\alpha}f^{\beta}\, RT[\frac{(X_B^{\beta} - X_B^{\alpha})}{X_B^{\gamma}(1 - X_B^{\gamma})}\, \Delta X_B^{e} \tag{17}$$

Equation (16) becomes

$$\frac{1}{S} = \frac{1}{S_o}\,[1 - \frac{\Delta X_B^{s}}{\Delta X_B^{e}}]$$

$$\frac{\Delta X_B^{s}}{\Delta X_B^{e}} = 1 - \frac{S_o}{S} \tag{18}$$

Substituting in equation (7)

$$v = \frac{2D\ \Delta X_B^{e}}{f^{\alpha}f^{\beta}(X_B^{\beta} - X_B^{\alpha})} \cdot \frac{1}{S}\,[1 - \frac{S_o}{S}] \tag{19}$$

The new quantity S_o is defined such that for $S \to S_o$ the growth rate v tends to zero. The value of S_o is not necessarily equal to S_c as defined previously by Zener [7], whereas S_c is related to the total available driving force which goes to surface energy as $S \to S_c$, the S_o is defined by equation (17).

Interface Diffusion-Controlled Theories: The extensive studies made on pearlite transformation in ferrous and non-ferrous alloy systems have indicated invariably that the observed growth rates are much larger to be explained by the volume diffusion-controlled mechanism. Though still not fully understood, the mechanism of diffusion of solute is believed to be proceeding along advancing interface. For example in case of steel, growth velocity as calculated was 0.16 μ/sec for ferrite while experimentally it came to be about 50 μ/sec.

The observed diffusivity is therefore three to four orders of magnitude higher than the value calculated from the volume diffusion mechanisms. By taking clue from the theory of cellular phase transformation, Turnbull [9] proposed interface controlled diffusion. However, the above discrepancy let Sundquist [11] to propose interface diffusion controlled growth of pearlite from austenite.

1.2.3 Turnbull's Treatment

While discussing the growth of discontinuous precipitation, Turnbull [9] suggested that the kinetics equation

proposed by Zener [7] for the eutectoid transformation could be modified to the case where growth rate is interface diffusion controlled. By substituting appropriate value for area of the interface through which solute transport occurs. Thus instead of $A^{\alpha} = S^{\alpha}.b$ in equation (5) the interface cross section $A^{\alpha} = 2b.\delta$ is used where δ is the interface thickness and factor of two is due to the fact that the solute is moving both sides of the α/γ interface. The diffusion distance is now taken S/4 instead of S^{α} to avoid dependence of S^{α} or S^{β} for a symmetric eutectoid. In addition to above modifications, distribution coefficient K is introduced, which is defined as the ratio of the solute in the interface and the bulk parent phase γ. Equation (5) then becomes

$$v = \frac{dm}{dt} = \frac{2bK\ D_b\delta}{V_m} \cdot \frac{\Delta X_B}{S/4} \qquad (20)$$

$$= \frac{8bK\ D_b\delta}{V_m S}\Delta X_B$$

The equation for growth then becomes

$$v = \frac{8K\ D_b\delta}{f^{\alpha}f^{\beta}(X_B^{\beta} - X_B^{\alpha})} \cdot \frac{1}{S^2}\left(1 - \frac{S_c}{S}\right) \qquad (21)$$

1.2.4 Sundquist's Treatment

Sundquist [11] has treated the growth of pearlite into austenite as a reaction that proceeds by diffusion of carbon in the advancing interface in plain carbon steels. His analysis includes the following implicit assumptions:

1. Interface diffusion is the dominant means of carbon transport.
2. The austenite to pearlite interface is curved as shown in Figure 9.
3. Local equilibrium exists across the advancing interface at every point along it i.e. at any position along the interface the chemical potential of solute is the same immediately on either side of that point.
4. The concentration of solute along the interface is not constant.

Darken and Fischer [3] proposed ferrite gap model as discussed previously. But with domination of interface diffusion mechanisms the ferrite gap model becomes indeterminant.

As in heat transfer problems, the rate of change of solute concentration at any point along the interface is given by

$$\frac{\partial C_b}{\partial t} = \frac{D_b\alpha}{V_m} \cdot \frac{\partial^2 X_B^b}{\partial y^2} + J_\alpha + J_\gamma$$

$$\frac{\partial C_b}{\partial t} = \frac{D_b\beta}{V_m} \cdot \frac{\partial^2 X_B^\beta}{\partial y^2} + J_\beta + J_\gamma$$

where

X_B^b = Solute concentration in the interface between γ and α, and γ and β of the pearlite. It is a function of distance along the interface.

y = Distance co-ordinate along the interface with the origin at the three phase junction.

Z = Distance co-ordinate perpendicular to the α/β interface with origin at the three phase junction.

$D_b\alpha$ = Grain boundary diffusivity along γ/α interface.

$D_b\beta$ = Grain boundary diffusivity along γ/β interface.

J_α, J_β, J_γ = Flux of solute from adjoining α, β, γ respectively to the grain boundary area.

Let V_y be the velocity of interface along normal to itself at any point along it and X_B^α, X_B^β, X_B^γ are solute concentrations in α, β and γ phases respectively far from the interface. Θ is the angle that normal to the interface forms with the growth direction.

Under steady state

$$\frac{\partial C_b}{\partial t} = 0 \tag{22}$$

$$J_\alpha = - \frac{V_y X_B^b}{\delta V_m}$$

$$J_\beta = - \frac{V_y X_B^\beta}{\delta V_m} \tag{23}$$

$$J_\gamma = \frac{V_y X_B}{\delta V_m}$$

and

$$V_y = V_X \cos\Theta \tag{24}$$

$$(V_X \cos\Theta)(X_B^\beta - X_B^\alpha) = - D_b\delta\left[\frac{\partial^2 X_B^b}{\partial y^2}\right] \tag{25}$$

For the requirement of local equilibrium at the interface the chemical potential of solute μ in the interface must be

equal to that in the austenite adjacent to the interface. It was further assumed that

$$X_B^b = K X_B^\alpha$$
$$X_B^b = K X_B^\beta \tag{26}$$

where K is a dimensionless constant.

Subdquist [11] calculated

$$X_B^\alpha = {}^\infty X_B^\alpha \left[1 + \frac{\beta_\alpha \gamma_\alpha}{RT} \frac{1}{r}\right] \tag{27}$$

where

β_α = Constant that can be evaluated for the α/γ interface.

γ_α = The interfacial energy of the α/γ interface.

r = The radius of curvature of the interface.

Solving these equations the following results have been obtained by Sundquist [11]:

$$U = \frac{3({}^oX_B^\alpha - {}^oX_B^\beta + R_\beta/L_\beta - R_\alpha/L_\alpha)}{(X_B^\gamma - X_B^\alpha)\frac{L^2\alpha}{RD} - (X_B^\gamma - X_B^\beta)L_\beta^2} \tag{28}$$

where

RD = $D_b\alpha/D_b\beta$

= Ratio of diffusivities of solute at γ/α interface to γ/β interface

$R_\alpha = ({}^oX_B^\alpha \beta_\alpha \gamma_\alpha \Theta_\alpha^o)/RT$

$R_\beta = ({}^oX_B^\beta \beta_\beta \gamma_\beta \Theta_\beta^o)/RT$

and

$U = V_X/(K\, D_b \delta)$

The plot of U with S gave the relation

$$US^3 = \text{Constant} \tag{29}$$

where $S \propto \frac{1}{\Delta T}$

where $\Delta T = T_e - T$

and $V_X \propto UD_b\alpha$

$$\propto (\Delta T)^3 D_b \alpha$$

or

$$V_X \propto (\Delta T)^3 \, \text{Exp}^{-Q/RT} \tag{30}$$

CHAPTER - 2

EXPERIMENTAL

Alloys for this investigation were prepared by melting together appropriate amounts of copper and indium (both of 99.99% purity) in sealed quartz tube under vacuum. In order to ensure homogeneity the quartz tubes were shaken a few times before solidification. Cylindrical rods, 8 mm diameter, thus obtained were homogenized for 8 days at 650°C (923 K). The average grain size of the β phase alloy containing 20.15 at. % In, balance copper, was approximately 500 μm. Disc specimens approximately 1.5 mm thick were cut from the cylinder using a diamond blade.

In order to study the kinetics of eutectoid transformation, alloy specimens were first solution treated at 620°C (893 K) for 10 minutes and then isothermally transformed in the temperature range 570-710 K. A number of specimens were transformed at each temperature for different length of time. All heat treatments were carried out in salt baths maintained within $\pm 2^{\circ}$ K of the desired temperature. The specimens were quenched in a mixture of ice and water maintained at 4°C (277 K).

The rate of growth of pearlite was determined by measuring the perpendicular distance from the original position of the grain boundary to the leading edge of the transformation front by utilizing optical microscopy. The interlamellar spacing measurements were made by utilizing optical

microscopy for higher transformation temperatures and scanning electron microscopy for the three lower transformation temperatures because the lamellae were fine at these low temperatures. A large number of measurements were made (40 or more) for both growth distance and lamellar spacing. All measurements were made only from those regions of the specimens where α and δ phases formed the lamellar structure.

CHAPTER - 3

RESULTS AND DISCUSSION

3.1 MORPHOLOGY

The microstructure observed through the optical and scanning electron microscope revealed that the β phase decomposed into α and δ phases at all transformation temperatures in the range 570 to 710 K. The transformation initiated at the grain boundaries and spread into grains from there. The transformation product progressed into both the grains, Figure 10. However, there were segments of the grain boundary or complete grain boundary regions where the growth occurred preferentially in one grain. The overall cooperative growth of the α and δ phases therefore is very similar to that observed during cellular phase transformation of the α solid solution of copper-indium alloys [17, 18], as represented by the optical photomicrograph of Figure 11 obtained during cellular phase transformation of a Cu - 8.9 at. % In alloy.

The pearlitic structure appeared to be lamellar with alternate lamellae of α and δ phases in agreement with the observation made by Mellor et al. [13] and Frebel et al. [14]. In certain regions of the specimen, Figure 12, a granular or granular like morphology was also observed as reported earlier [12]. On carefully tilting under the scanning electron microscope, it was observed that the

granules were slightly elongated. It is appropriate to call such a structure as segmented rods aligned along a straight line. The rods (however of small length) appeared as granular when lying perpendicular to the specimen surface. The extent of growth on each boundary was not the same in agreement with the cellular phase transformation in this alloy system. Assuming interface controlled transformation, this is expected because the interface mobility is directly related to the structure and degree of disorder of such interfaces. The similarity in the behaviour of the eutectoid and cellular phase transformations in the Cu-In alloy system was to the extent that the transformation was not initiated on a small fraction of the grain boundary which in the case of later transformation is due to Smith's criterion [2]. Accordingly, nucleation on the grain boundaries having angle of misorientation of less than 11^{o} does not occur or occurs very late in the transformation process.

3.2 GROWTH RATE

The growth rate of pearlite was determined by measuring growth distance as a function of the time of transformation. Growth distance was measured from the original position of the grain boundary to the leading edge of the transformed region. Since the growth distance varied from boundary to boundary and some times on adjacent segments of the same grain boundary, a large number of measurements were made (approximately 40) from different regions of the same specimen. The data were averaged and multiplied by a factor

$\pi/4$ to be consistent with the bulk averaging technique of Gust et al. [19] used during study of the kinetics of cellular phase transformation. The growth distance data presented in Figure 13 vs. time at a few temperatures indicate a linear behaviour. The growth rate was calculated from the best straight line drawn through the points and is presented in Figure 14. The growth rate is observed to increase with increasing temperature. At the highest temperature, 710 K, used in this study, the growth rate is still increasing. However, from the trend of the growth rate vs. temperature curve, it appears that the growth rate would reach a maximum and then decreases indicating a C-curve or near C-curve behaviour typical of the pearlite transformation. Since no isothermal growth rate data on the Cu-In system is available, a direct comparison could not be made. However, a comparison with the cellular phase transformation in Cu-In alloy system reveals that whereas the growth rate of the secondary cellular transformation is comparable to the present result of eutectoid transformation, the rate of growth of the primary cells is approximately an order of magnitude higher. A lower rate of growth of the product of the eutectoid transformation is expected from the complete partitioning of solute as will become apparent from the composition of the α phase.

3.3 INTERLAMELLAR SPACING

The interlamellar spacing, S, measurements were made only from those regions of the specimen where abundance

of the lamellar structure was observed. About 40 measurements were made from different regions of the specimen at each temperature. The data were averaged and multiplied by a factor $\pi/4$. The interlamellar spacing vs. temperature is plotted in Figure 15. A comparison with the cellular phase transformation in this system reveals that the interlamellar spacings of pearlite are higher than those of the primary cells, however, they are comparable with the secondary cells. This is consistent with the growth rate results. In order to determine the functional relationship between S and ΔT, the interlamellar spacing data were plotted on a log-log scale, Figure 16. Within the error of the experiment, the data fall on a straight line. The slope of the average line is -1, which gives a relation of the type $S \propto (\Delta T)^{-1}$ typical of the pearlite transformation in eutectoid steel [20]. In order to verify the reported eutectoid transformation temperature in this alloy, the reciprocal of the interlamellar spacing was plotted against the absolute transformation temperature, Figure 17. Extrapolation of the data to $1/S = 0$ gives a value of T_E (= 843 K) at which the interlamellar spacing becomes infinite. This is within 4 K of the reported eutectoid transformation temperature of 847 K thus in good agreement.

3.4 COMPOSITION OF THE α PHASE

The composition of the α phase of the pearlite was measured using X-ray diffraction. The 2θ value of the {220}

peak was monitored using CuK_α radiation and a Ni-filter. The 2θ values were corrected for instrumentation error by determining the 2θ peak position of the {220} peak for well annealed high purity (99.999%) Cu. The composition of the α phase was determined from the lattice parameter-composition data presented by Subramanian et al. [21]. The compositions of the α phase are presented in Figure 18 along with the equilibrium solvus (α). The composition values match very well with the equilibrium phase diagram especially at higher temperatures. There is a small departure at lower temperatures. In comparison, the depleted matrix of the primary cells of the cellular phase transformation in a Cu - 8.9 at. % In alloy are richer in solute at all aging temperatures. It is predicted therefore that the solute partitioning is complete during eutectoid transformation and is reflected in the lower rate of growth of pearlite in this alloy system.

3.5 TRANSFORMATION KINETICS

A number of theories have been proposed in the past to describe the kinetics of eutectoid transformation in alloys. Based on the diffusion mechanism controlling the transformation, these theories can be divided into two groupsl the interface diffusion controlled and volume diffusion controlled. Hillert[22] has described Zener's [7] treatment of eutectoid transformation and pointed out that Zener [7] was the first to take surface effects into

consideration in his mathematical treatment. The reaction proceeds under the available driving force, a part of which is associated with the α/δ interface of the lamellar structure. Accordingly, the growth rate of the eutectoid transformation is given by

$$v = \frac{2D}{f^{\alpha} f^{\delta}} \cdot \frac{\Delta X_B^e}{(X_B^{\delta} - X_B^{\alpha})} \cdot \frac{1}{S}\left(1 - \frac{S_c}{S}\right) \qquad (10)$$

In equation (10), D is the volume diffusivity of solute in the β phase, f^{α} and f^{δ} are the fractions of α and δ phases respectively, ΔX_B^e is the difference in the interface compositions between β/α and β/δ interfaces, and S_c is the critical spacing at which the growth rate is zero. Hillert [22] modified the growth rate expression, equation (10), by introducing the effect of interface shape on solute concentration and the interface compositions. Accordingly,

$$v = \frac{2D}{f^{\alpha} f^{\delta}} \cdot \frac{\Delta X_B^e}{(X_B^{\delta} - X_B^{\alpha})} \cdot \frac{1}{S}\left(1 - \frac{S_o}{S}\right) \qquad (19)$$

Equations (10) and (19) are similar except for S_o replacing S_c in equation (19) . S_o is expressed by

$$\frac{2\gamma V_m}{S_o} = f^{\alpha} f^{\delta} RT \frac{(X_B^{\delta} - X_B^{\alpha})}{X_B^{\beta}(1 - X_B^{\beta})} \Delta X_B^e \qquad (17)$$

The kinetic equation proposed by Zener [7] for the volume diffusion controlled transformation was modified by Turnbull [9] by considering the transport of solute through the interface. This has been done by substituting appropriat

value of the area through which diffusion occurs ($A = 2b\delta$) and the thickness of the interface region, δ. Thus, the growth rate is

$$v = \frac{8KD_b\delta \ \Delta X_B^e}{f^\alpha f^\delta (X_B^\delta - X_B^\alpha)} \cdot \frac{1}{S^2}\left(1 - \frac{S_c}{S}\right) \qquad (21)$$

In equation (21), K is the segregation ratio of solute in the matrix and the interface. Growth of pearlite under boundary diffusion control of the solute has been considered by Hillert [23] who proposes that

$$v = \frac{12KD_b\delta \ \Delta X_B^e}{f^\alpha f^\delta (X_B^\delta - X_B^\alpha)} \cdot \frac{1}{S^2}\left(1 - \frac{S_c}{S}\right) \qquad (31)$$

Equations (21) and (31) are similar except for the factor 12 in equation (31) in place of 8. Sundquist [24] considered pearlite growth to be edge-wise and wrote the differential equation at both β/δ and β/α interfaces. The parameter U defines the growth rate, V_X, in the forward direction is given as

$$U = \frac{V_X}{KD_b\delta}$$

The parameter U is related to S by US^3 = Constant, which yields

$$V_X S^3 = \text{Constant}(KD_b\delta) \ \ \text{Exp}^{-Q/RT} \qquad (32)$$

Considering a number of similarities between the cellular phase transformation and the eutectoid transformation

in these alloys, the boundary diffusion controlled theory of Petermann and Hornbogen [25] as applied to cellular phase transformation can be extended in analysing the results of the eutectoid transformation. Accordingly,

$$v = \frac{8KD_b\delta\ \Delta G}{S^2\ RT} \tag{33}$$

where ΔG is the effective driving force, related to the total available driving force, ΔG_o, and the interfacial energy as,

$$\Delta G = \Delta G_o + \frac{2\gamma\ V_m}{S} \tag{2}$$

where γ is the specific interfacial energy of the α/δ interface taken to be 0.4 J m^{-2} [14] and V_m is the molar volume (= 8.2454 X 10^{-6} m^3 mol^{-1}).

The experimentally observed growth rate, v, interlamellar spacing, S, and composition values of the α phase were recorded at each transformation temperature as shown in Sections 3.2 to 3.4. ΔX_B^e values were calculated by extrapolating the β/α and β/δ phase boundaries to the transformation temperatures. The composition of the δ phase, X_B^δ, varies from 0.29 to 0.306. A convenient value of X_B^δ = 0.3 was used throughout the analysis. The calculation of the total driving force posed few problem because of the insufficient information on the entropy of formation of the β phase. However, this was overcome by using the relation

$$\Delta G_o = \frac{\Delta H_m\ .\ \Delta T}{T_e} \tag{35}$$

where ΔH_m is the enthalpy of the reaction $\beta \rightarrow \alpha + \delta$, ΔT is the difference in the eutectoid, T_e, and the transformation temperature. The total available driving force, ΔG_o, was also calculated using an approximate equation (36) suggested by Hillert [22] and is presented in Table 2 at each temperature. The total driving force is given as follows

$$\Delta G_o = \frac{\Delta X_B^e \, RT \, f^{\alpha} f^{\delta} (X_B^{\alpha} - X_B^{\delta})}{X_B^{\beta}(1 - X_B^{\beta})} \qquad (36)$$

The ΔG_o values calculated using equation (35) is three to four times the value obtained using equation (36) at each temperature. However, both values are used in the analysis to obtain the range of diffusivity values after the model of Petermann and Hornbogen [25].

Using the experimental or calculated values of the various quantities in the preceding paragraphs, the diffusivities, ($KD_b\delta$ or D) were calculated at each transformation temperature for the volume diffusion controlled model after Hillert [22] and interface diffusion controlled model after Turnbull [9], Sundquist [24], Hillert [23] and Petermann and Hornbogen [25]. The diffusivities thus calculated are plotted against the reciprocal of absolute temperature in an Arrhenius plot shown in Figures 19, 20 and 21. There is some scatter in the data however, within the error of the experiment the data points can be represented to fall on straight lines in each case.

There is a general lack of information in the literature about the grain boundary diffusivity for the diffusion

of In in Cu. However, from the work of Hoshino et al. [26] on the lattice diffusion coefficient of In in Cu in dilute Cu-In alloys, the order of magnitude of the diffusivity in the α/α phase boundary may be calculated. If it is assumed that the activation energy for grain boundary diffusion is one-half to two-thirds of the regular lattice diffusion value, then Q_b is expected to lie in the range 100 to 133 kJ mol^{-1}. Using these values and $D_o = 0.6 \times 10^{-4}$ m^2 s^{-1} from the work of Hoshino et al. [26], the grain boundary diffusivity ($KD_b\delta$) is expected to fall in the range 10^{-23} to 10^{-26} m^3 s^{-1} at 650 K, for $\delta = 5 \times 10^{-10}$ m. The cell boundary diffusivity values are 6.7×10^{-22} m^3 s^{-1} and 1.65×10^{-22} m^3 s^{-1} for the primary and secondary cell growth respectively during cellular phase transformation using Petermann and Hornbogen [25] analysis of the grain boundary diffusion controlled transformation. The diffusivity obtained in the present investigation falls in the range 1×10^{-22} to 3×10^{-22} m^3 s^{-1} at 650 K. The volume diffusivity, D, at this temperature is 5.07×10^{-21} m^2 s^{-1} which when multiplied by the boundary thickness, δ, for comparison purpose only, yields $D\delta$ to be $2.53 \times 10^{-30} m^3$ s^{-1}. This is seven orders of magnitude lower than the boundary diffusivity.

The diffusivity of In in β Cu-In alloys for the β/α and β/δ interfaces can be obtained from the work of Mellor and Chadwick [27]. From the rate of displacements of the $\beta/(\beta + \alpha)$ and $\beta/(\beta + \delta)$ interfaces in a diffusion couple experiment, they have reported Q_V to be 330 ± 80 kJ

mol^{-1} and D_o = 5.7 X 10^{8} m^2 s^{-1}. The diffusivity of In for the displacement of $\beta/(\beta + \delta)$ interface is of the same order of magnitude, but slightly lower. The volume diffusivity of In in β Cu-In alloys for the growth of α/β interface is 1.72 X 10^{-18} m^2 s^{-1} at 650 K, which when multiplied by δ yields $D\delta$ = 8.6 X 10^{-28} m^3 s^{-1}. The volume diffusivity of In in the β phase is four to five orders of magnitude lower than the experimentally observed diffusivity at 650 K for interface controlled transformations.

Comparing the volume diffusion value for the diffusion of In in β Cu-In alloys with the volume diffusion controlled transformation after Hillert [22], it is apparent that the observed diffusivity is two orders of magnitude higher at 650 K. The difference increases to four orders of magnitude at lower temperatures only at the highest temperature of transformation used in this study, the calculated value is comparable to that observed. It is tempting to conclude that the volume diffusion of In plays a significant role during eutectoid transformation of β Cu-In alloys especially at higher temperatures. However, the activation energy of 110 kJ mol^{-1} is approximately one-third the reported value of 330 kJ mol^{-1}. The volume diffusion controlled transformation of β Cu-In alloys can be safely ruled out. The same conclusion can be arrived at from the volume diffusivity of In in Cu for the growth of β/δ interface.

Considering the interface diffusion controlled transformation, the activation energy for the diffusion of

in for $\rho/(\alpha + \beta)$ interface migration is approximately 330/2(= 165) kJ mol^{-1}. Interface diffusivity of In $KD_b\delta$, is 2.7 X 10^{-23} m^3 s^{-1} at 650 K. This value is well within an order of magnitude of the observed diffusivity for the model after Petermann and Hornbogen [25] and comparable with values of 1.7 X 10^{-23} and 1.135 X 10^{-23} m^3 s^{-1} observed for the interface controlled models after Turnbull [9] and Hillert [23] respectively.

Comparing the present result with those of cellular phase transformation in a Cu - 8.9 at. % In alloy, the diffusivity values lie well within those observed for the growth of primary and secondary cells for the theory of Petermann and Hornbogen [25]. Since the cellular phase transformation and discontinuous coarsening of the cellular precipitate occurs by solute transport through the grain boundary it can be concluded that a similar high diffusivity path of In diffusion through the interface is responsible for the growth of pearlite in the Cu-In alloy. The boundary diffusivity of In in Cu for both α/α and α/β interfaces is expected to be of the same order of magnitude.

From the Arrhenius plot, the activation energy was calculated for each theory. Considering the diversity of approach of different interface controlled theories of the pearlite transformation, the activation energy values are in excellent agreement, Table 3. The activation energies are within $\pm$5 kJ mol^{-1} of 130 kJ mol^{-1}. This is more than half the lower bound value of 125 kJ mol^{-1} estimated for the grain boundary diffusion of In in β Cu-In alloys. It can

be concluded therefore that the pearlite transformation in β Cu-In alloys occurs by interface diffusion controlled mechanism.

3.6 MOBILITY AND CHEMICAL FREE ENERGY

The chemical free energies used in analysing the eutectoid transformation is plotted in Figure 22 vs. the transformation temperature. The chemical free energy increases with decreasing transformation temperature. The interfacial free energy is small in comparison. The chemical free energy available to drive the eutectoid transformation is higher than that available during cellular phase transformation as shown in Figure 23 for comparison.

The analysis of the pearlite transformation can be extended by assuming a mobility controlled transformation. Assuming a linear relationship to describe the interface boundary migration we can write for cell growth,

$$M = - \frac{v V_m}{\Delta G} \qquad (37)$$

where M is the mobility expressed as velocity per unit force. The mobilities were calculated using equation (37) as shown in Figure 22. The activation energies for the mobility controlled transformation are 95.8 and 92.5 kJ mol^{-1} for the two sets of ΔG values obtained through equations (35) and (36) respectively. The activation energy calculated for the growth of cells during cellular phase transformation in a Cu - 8.9 at. % In alloy is 95.8 which

is in excellent agreement with results of the present investigation. The mobility of the α/β interface appears to be lower than the mobility of the α/α interface obtained during cellular phase transformation although the kinetic processes involved are the same.

CONCLUSIONS

Copper-indium alloy of the eutectoid composition decompose into α and δ phases when transformed in the temperature range 570-710 K. The product of the transformation is lamellar in nature although granular structure consisting of short segmented rods also occupies a substantial part of the overall structure. There is substantial experimental evidence to suggest that the growth of pearlite occurs by the diffusion of indium through the α/β interface. Both diffusivity and activation energy suggest an interface diffusion controlled transformation. Upon comparison with the cellular phase transformation and discontinuous coarsening of the cellular precipitation in Cu-In alloy system (8.9 at. % In) it is apparent that during eutectoid transformation the growth rate, interlamellar spacing and composition of the α phase are closer to the result obtained during discontinuous coarsening reaction although the available driving force is quite high. This may be due to lower mobility of the α/β interphase compared to the α/α interface during cellular transformation.

REFERENCES

1. C.J. Benedicks, J. Iron Steel Inst. (London), 2, 352 (1905).

2. C.S. Smith, Trans. ASM, 45, 533 (1953).

3. L.S. Darken and R.M. Fisher, Decomposition of Austenite by Diffusional Processes, Met. Soc., AIME, 549 (1962).

4. M. Hillert, Decomposition of Austenite by Diffusional Processes, Met. Soc. AIME, (1962).

5. W.H. Brandt, J. Appl. Phy. 16, 139 (1945).

6. E. Scheil, Z. Metallkde. 37, 123 (1946).

7. C. Zener, AIME Trans. 167, 550 (1946).

8. M. Hillert, Jern. Kont. Ann. 141, 757 (1957).

9. D. Turnbull, Acta Metall. 3, 55 (1955).

10. J.W. Cahn, Acta Metall. 7, 18 (1959).

11. B.E. Sundquist, Acta Metall. 16, 1413 (1968).

12. C.W. Spencer and D.J. Mack, Decomposition of Austenite by Diffusional Processes, Met. Soc. AIME, 549 (1962).

13. B.G. Mellor and G.A. Chadwick, Metal Sci. 6, 65 (1974).

14. M. Frebel and G. Duddek, Mat. Sc. Eng. 32, 17 (1978).

15. M. Kaya and R.W. Smith, Acta Metall. 37, 1667 (1989).

16. J.D. Livingston and J.W. Cahn, Acta Metall. 22, 495 (1974).

17. S.P. Gupta, Acta Metall. 34, 1279 (1986).

18. R.A. Fournelle and J.B. Clark, Metall. Trans. 3, 2757 (1972).

19. W. Gust, M.B. Hintz, R. Lucic and B. Predel, Mater. Res. Soc. Symp. Proc. 21, 513 (1983).

20. D. Brown and N. Ridley, J. Iron Steel Inst. 207, 1232 (1969).

21. P.R. Subramanian and D.E. Laughlin, Bull. Alloy Phase Diagrams, 19, 554 (1989).

22. M. Hillert, Metall. Trans. 3, 2729 (1972).

23. M. Hillert, The Mech. of Phase Trans. in Cryst. Solids, Inst. Metals London, Manchester, 231 (1969).

24. B.E. Sundquist, Acta Metall. 16, 1413 (1968).

25. J. Petermann and E. Hornbogen, Z. Metallk. 59, 814 (1968).

26. K. Moshino, Y. Iijiyama and K. Hirano, Acta Metall. 30, 265 (1982).

27. B.G. Mellor and G.A. Chakwick, Metal. Sci. 8, 63 (1974).

Table 1. Growth rate, interlamellar spacing and composition of the α phase.

T, K	v, ms^{-1} ($\times 10^{-10}$)	S, m ($\times 10^{-7}$)	X_B^α	$e_{X_B^\alpha}$
710	14.8	7.238	0.0405	0.0407
690	10.5	5.662	0.0301	0.03075
670	7.44	5.076	0.024	0.024
650	4.95	4.596	0.01925	0.0195
630	3.13	4.091	0.0158	0.0165
610	1.84	3.765	0.013	0.0145
590	1.05	3.52	0.0095	0.013
570	0.4	3.16	0.008	0.012

Table 2. Calculated values of the driving force.

	Equation (35)		Equation (36)		
T, K	ΔG_o	ΔG	ΔG^{γ}	ΔG_o	ΔG
710	474.6	465.5	9.11	152.36	143.25
690	566.38	554.73	11.65	173.22	161.57
670	654.68	641.68	13.0	193.98	180.98
650	740.16	725.81	14.35	210.82	196.47
630	825.43	809.31	16.12	225.1	208.98
610	909.68	892.16	17.52	237.56	220.04
590	997.28	978.54	18.74	250.86	232.14
570	1079.81	1058.94	20.87	261.7	240.83

Table 3. The activation energy and $(KD_b\delta)$ values for different models. The activation energy for mobility controlled transformation is also shown.

	Hillert volume diffusion	Turnbull	Hillert	Sundquist	Petermann and Hornbogen		Mobility	
$KD_b\delta)_o$ ^{3} mol^{-1}	$5.69X10^{-8}$	$4.52X10^{-13}$	$3.01X10^{-13}$	-	$7.22X10^{-12}$ Eq. (35)	$1.14X10^{-11}$ Eq. (36)	- Eq. (35)	- Eq. (36)
, ^{3} mol^{-1}	110.25	129.8	129.8	130.8	135	130.5	95.8	92.5

Fig. 1. Optical photomicrograph showing structure of pearlite on one side of the grain boundary and bainite on the other side of the same grain boundary.

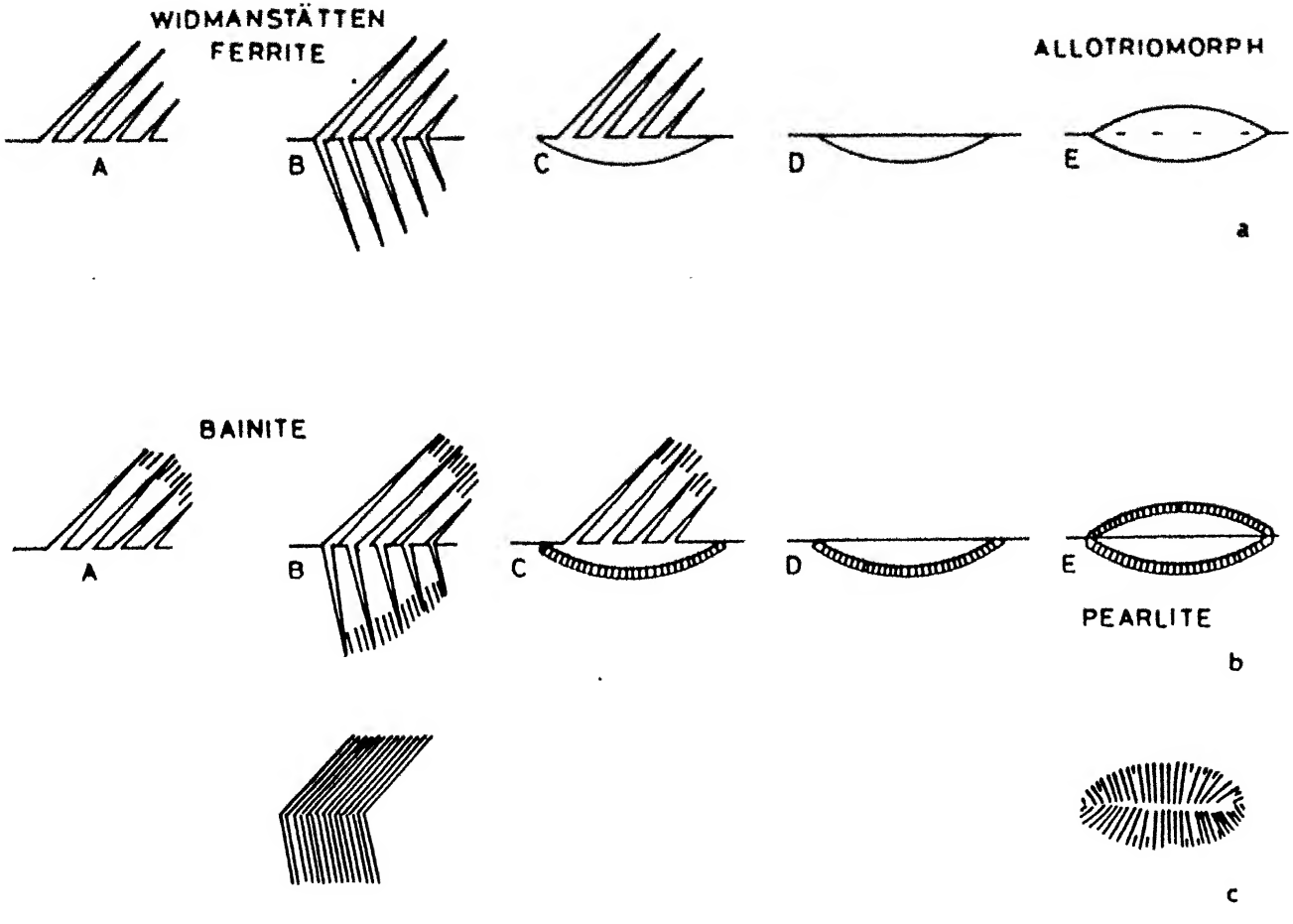

Fig. 2. Schematic diagram showing structure morphology depending upon the orientation relationship between parent and product phase.

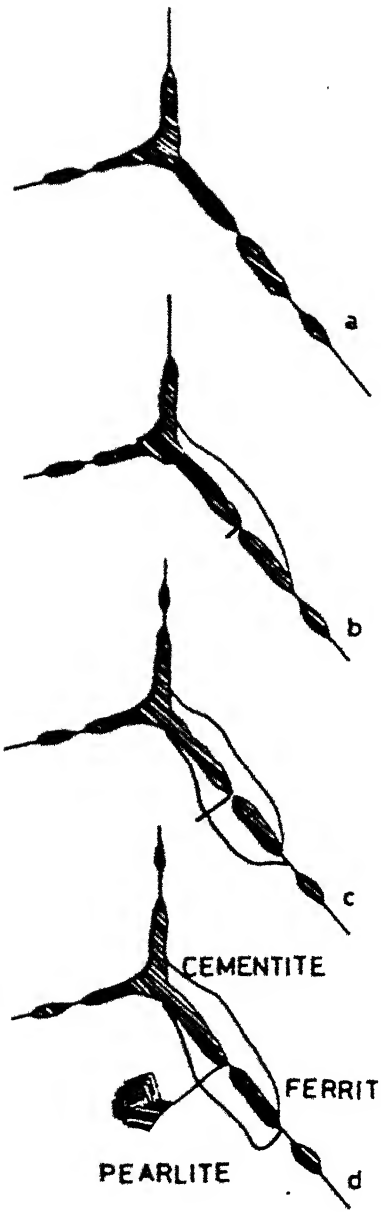

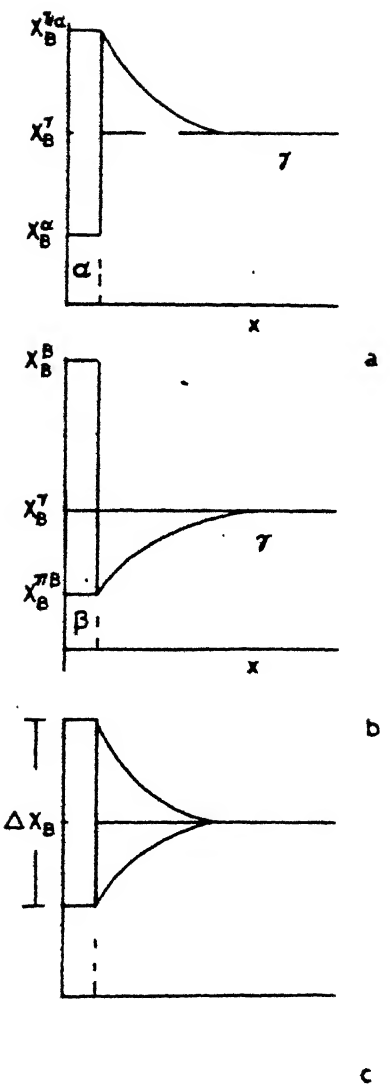

Fig. 3. Formation of pearlite.

Fig. 4 & 5. Concentration gradient developed due to precipitation of ferrite and cementite on grain boundary.

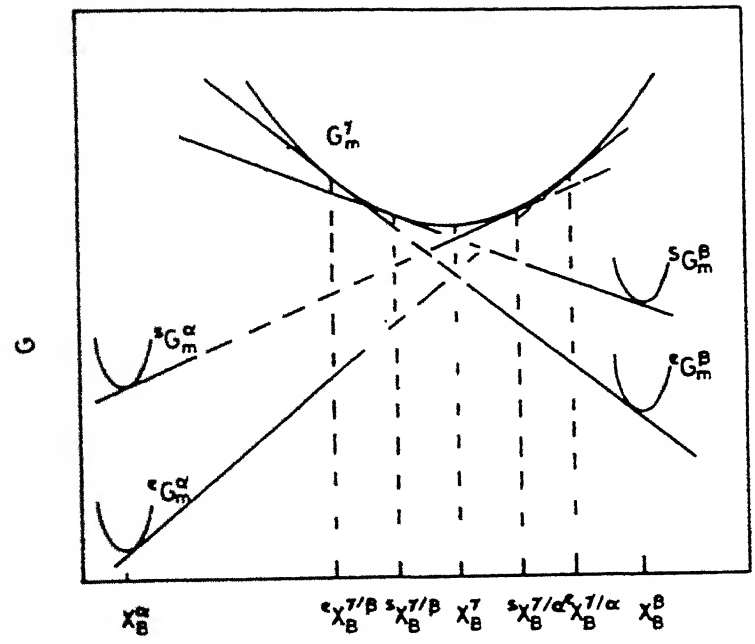

Fig. 6. Free energy-composition diagram.

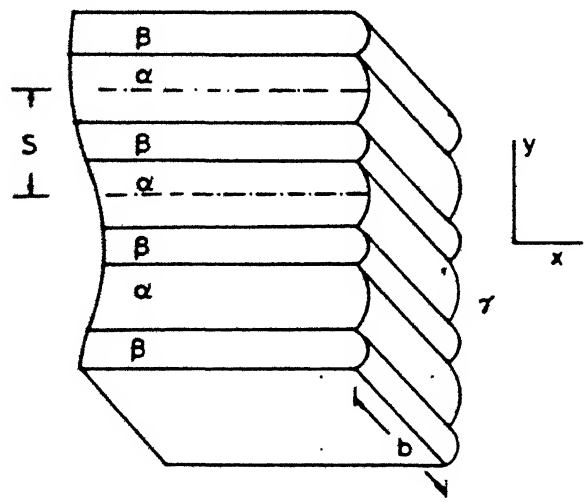

Fig. 7. Lamellar structure of pearlite-Zener's model.

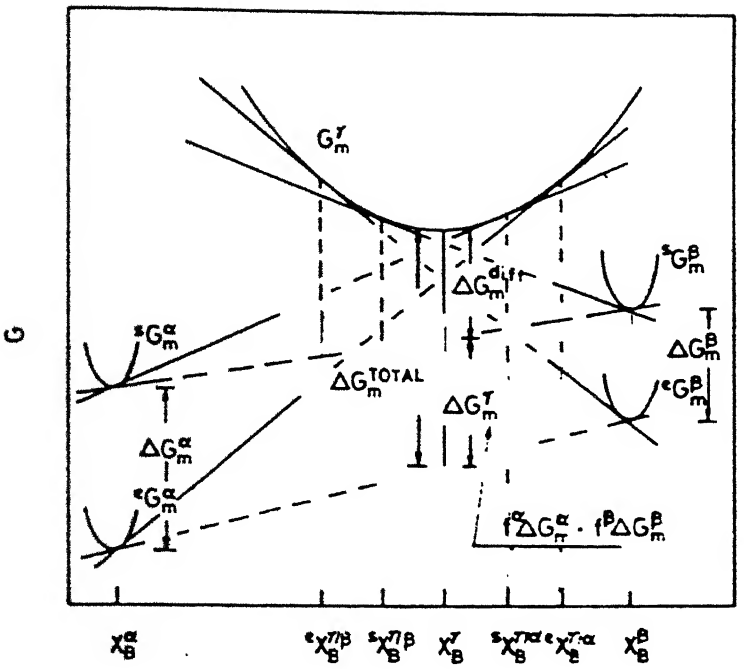

Fig. 8. Free energy-composition diagram - Hillert's model.

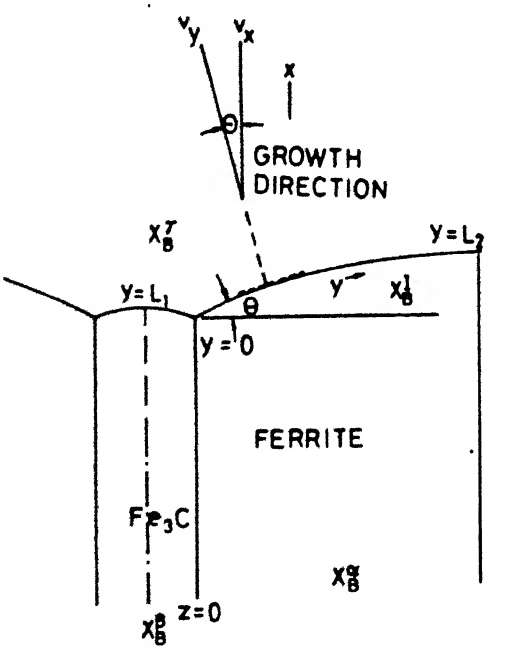

Fig. 9. Curved interface between parent and product phase - Sundquist's model.

Fig. 10. Optical photomicrograph showing structure of pearlite on grain boundaries, specimen transformed for h at 710 K.

Fig. 11. Optical photomicrograph showing structure during cellular phase transformation in a Cu - 15 wt. % I alloy specimen aged for 8.5 h at 665 K.

Fig. 12. Optical photomicrograph showing the lamellar structure of pearlite, specimen transformed for h at 710 K.

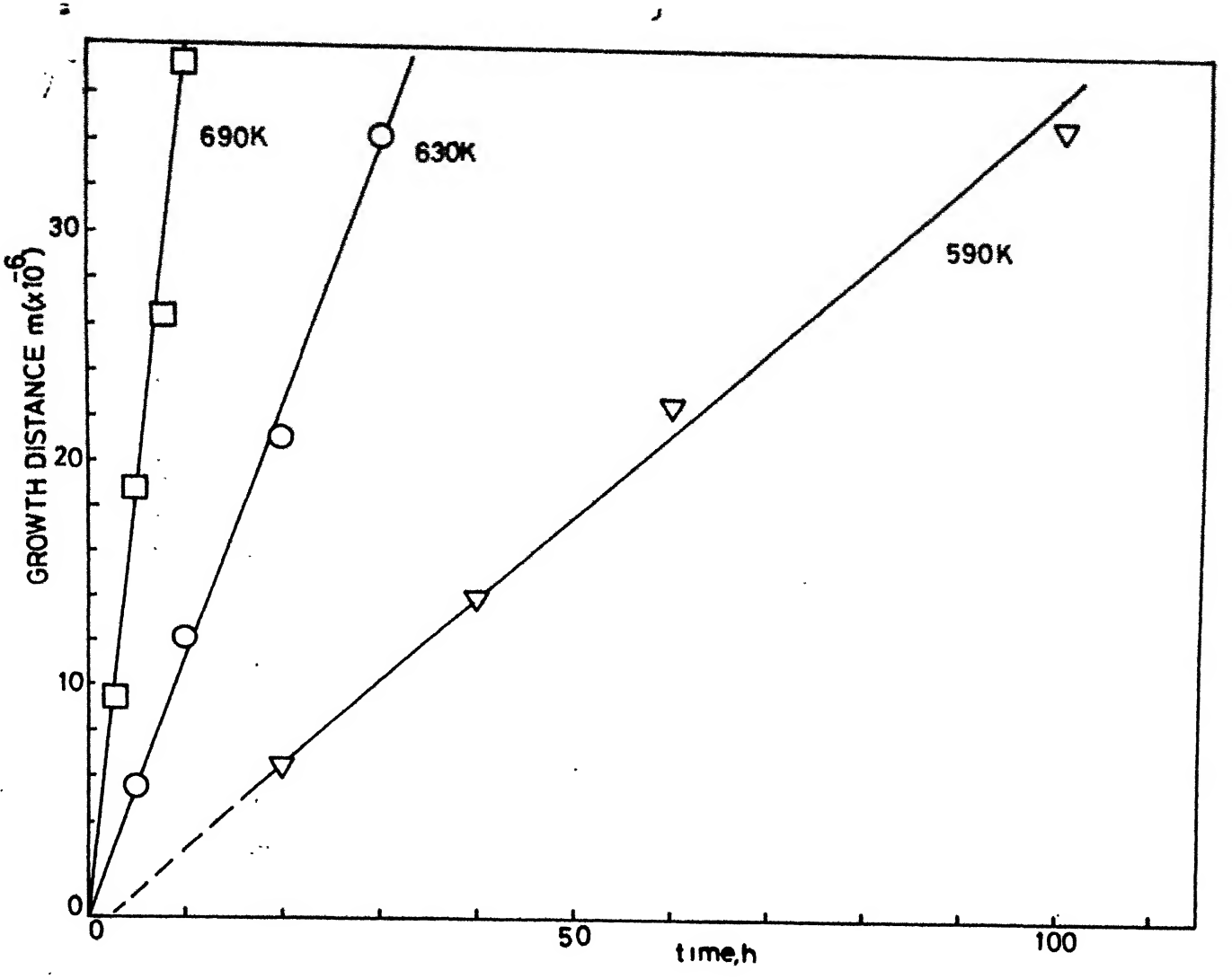

Fig. 13 The growth distance vs. time.

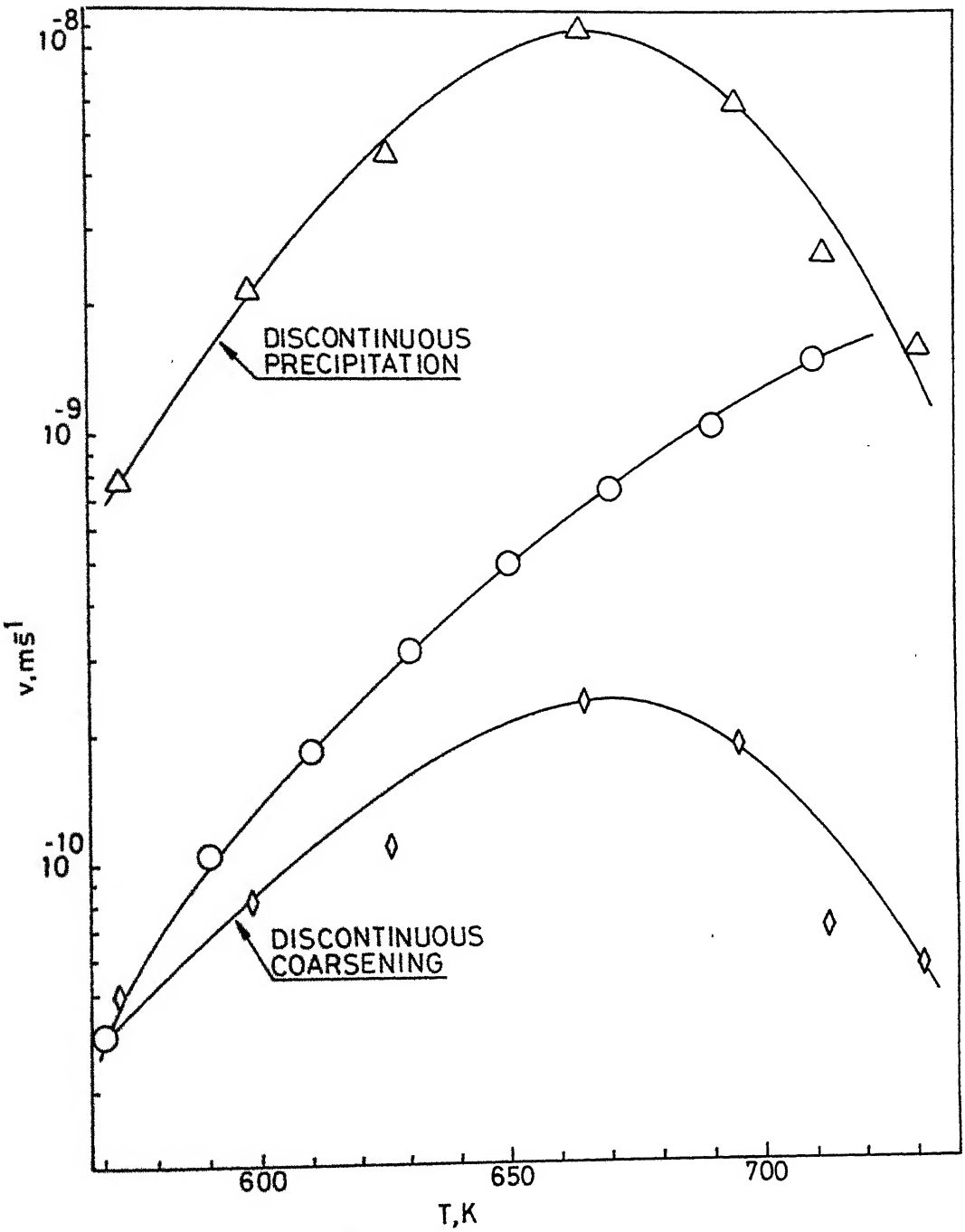

Fig. 14. The growth rate of pearlite vs. temperature. The growth rate obtained during discontinuous precipitation and discontinuous coarsening of the cellular precipitate obtained in a Cu - 15 wt. % In alloy are also shown for comparison.

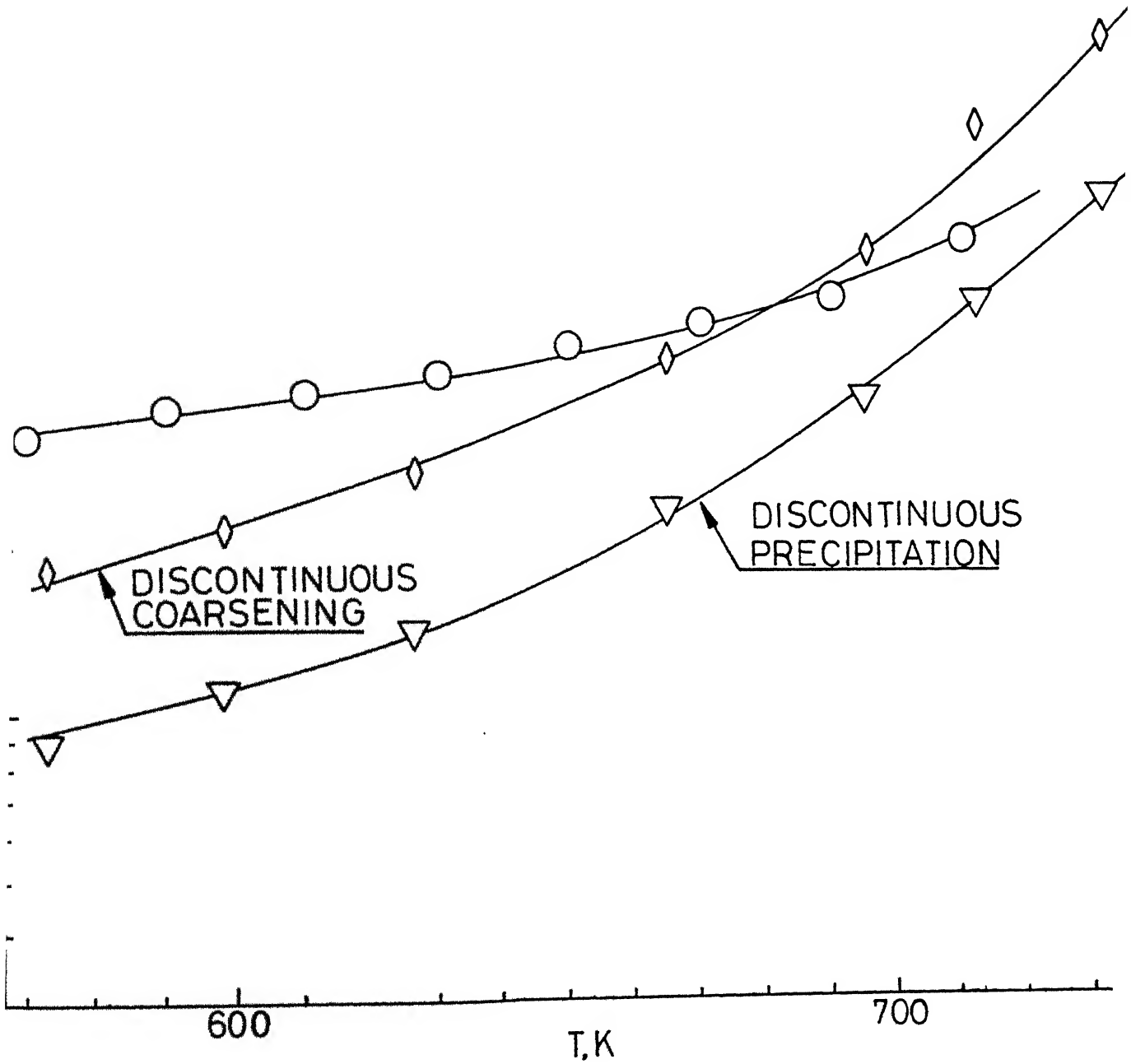

Fig. 15. The interlamellar spacing vs. temperature. The interlamell spacing data obtained during discontinuous precipitation a discontinuous coarsening of the cellular precipitate obtai in a Cu - 15 wt. % In alloy are also shown for comparison.

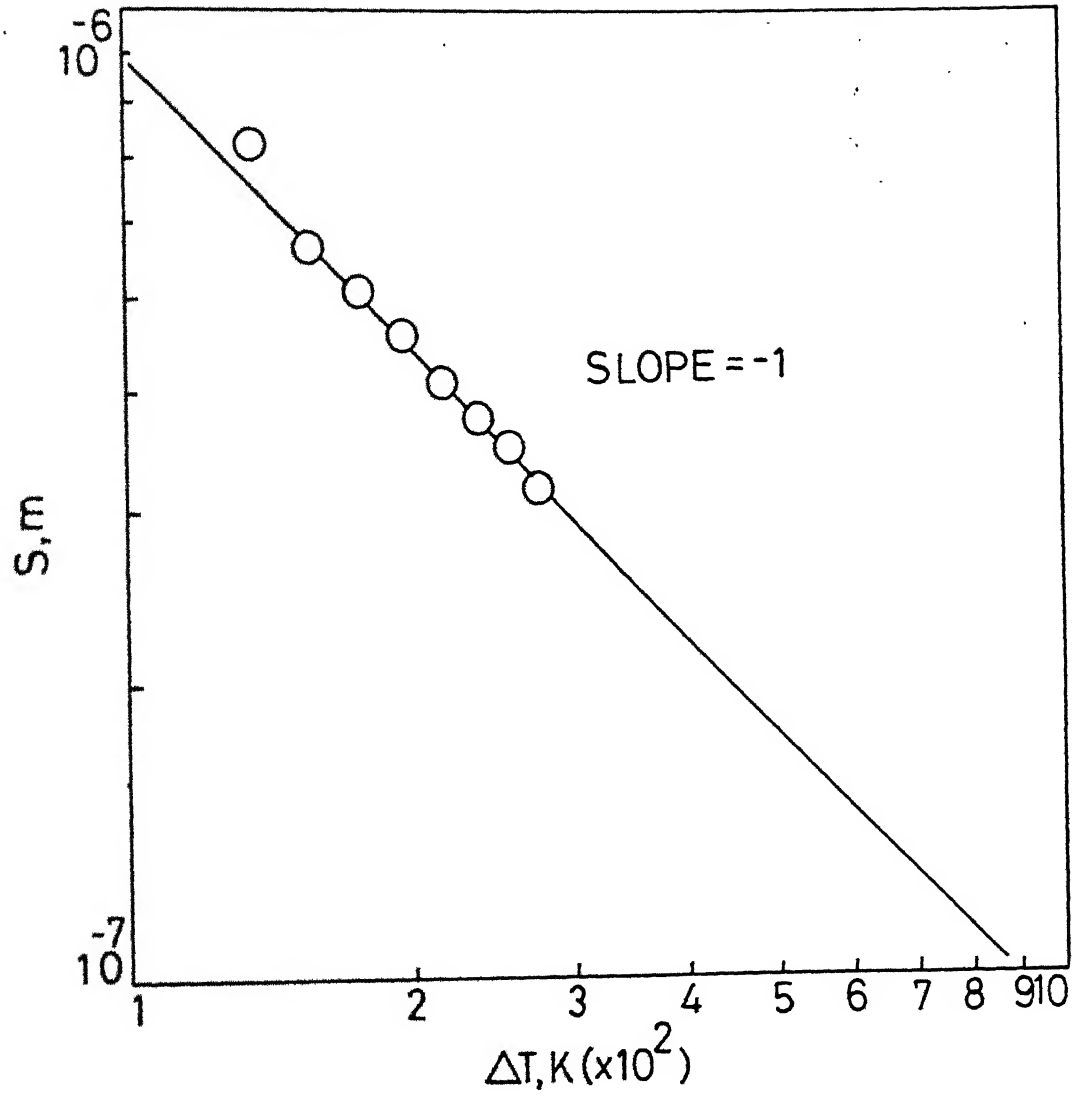

Fig. 16. S vs. ΔT plotted on a log-log scale.

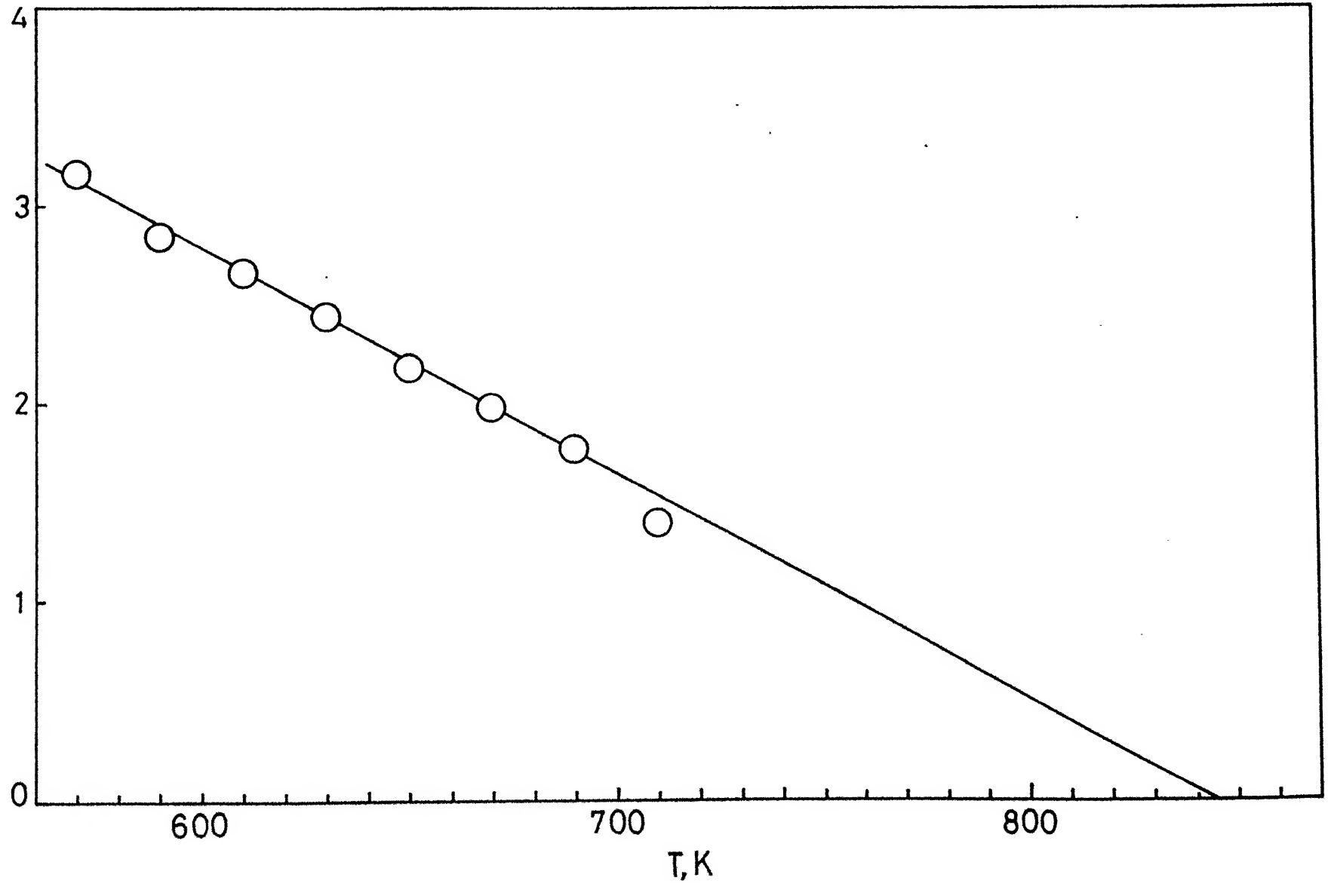

Fig. 17. 1/_ vs. T, extrapolation of the line yields T_E = 843 K.

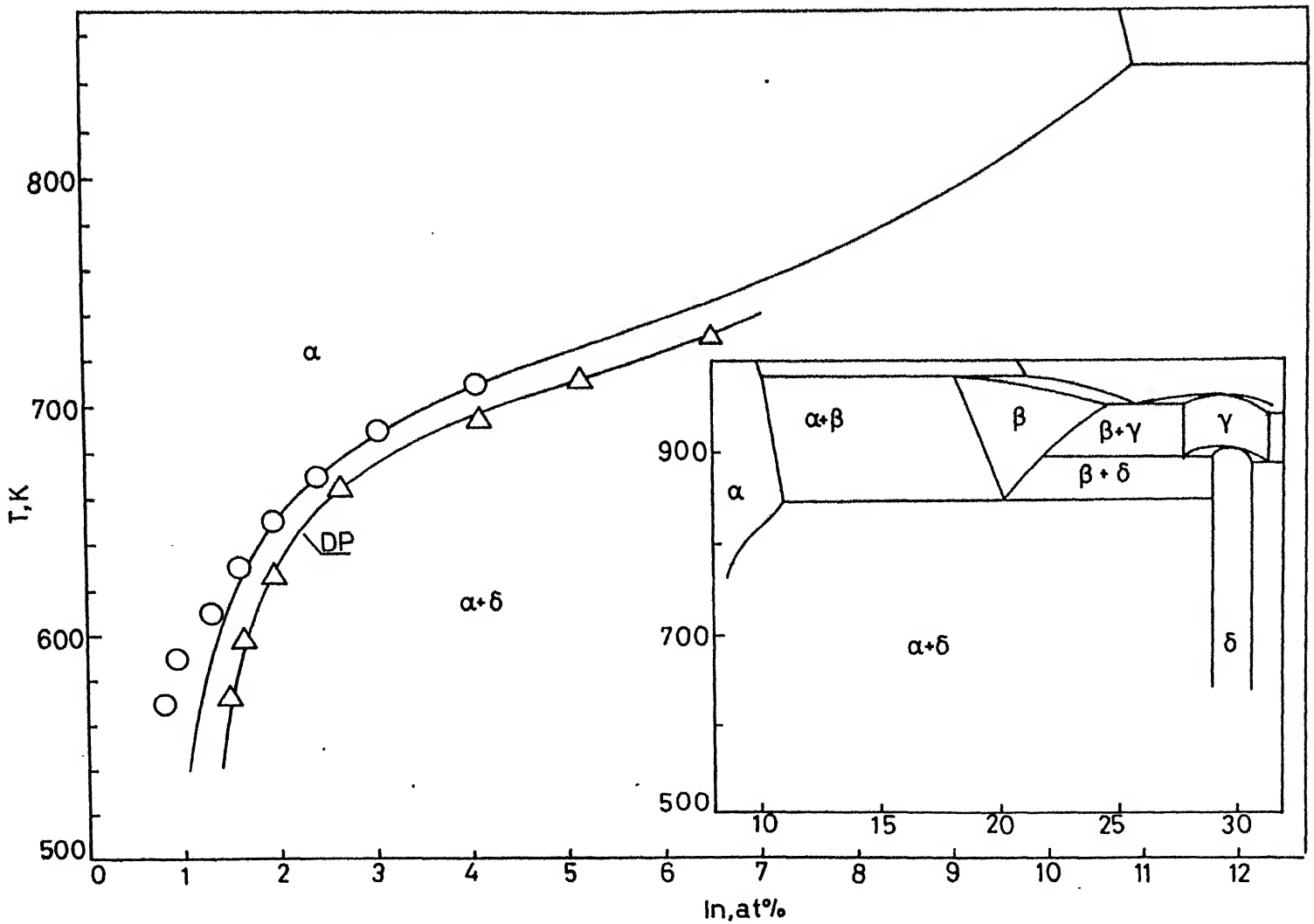

Fig. 18 The Cu-In phase diagram and composition of the α phase in equilibrium with δ during eutectoid transformation and discontinuous precipitation (DP).

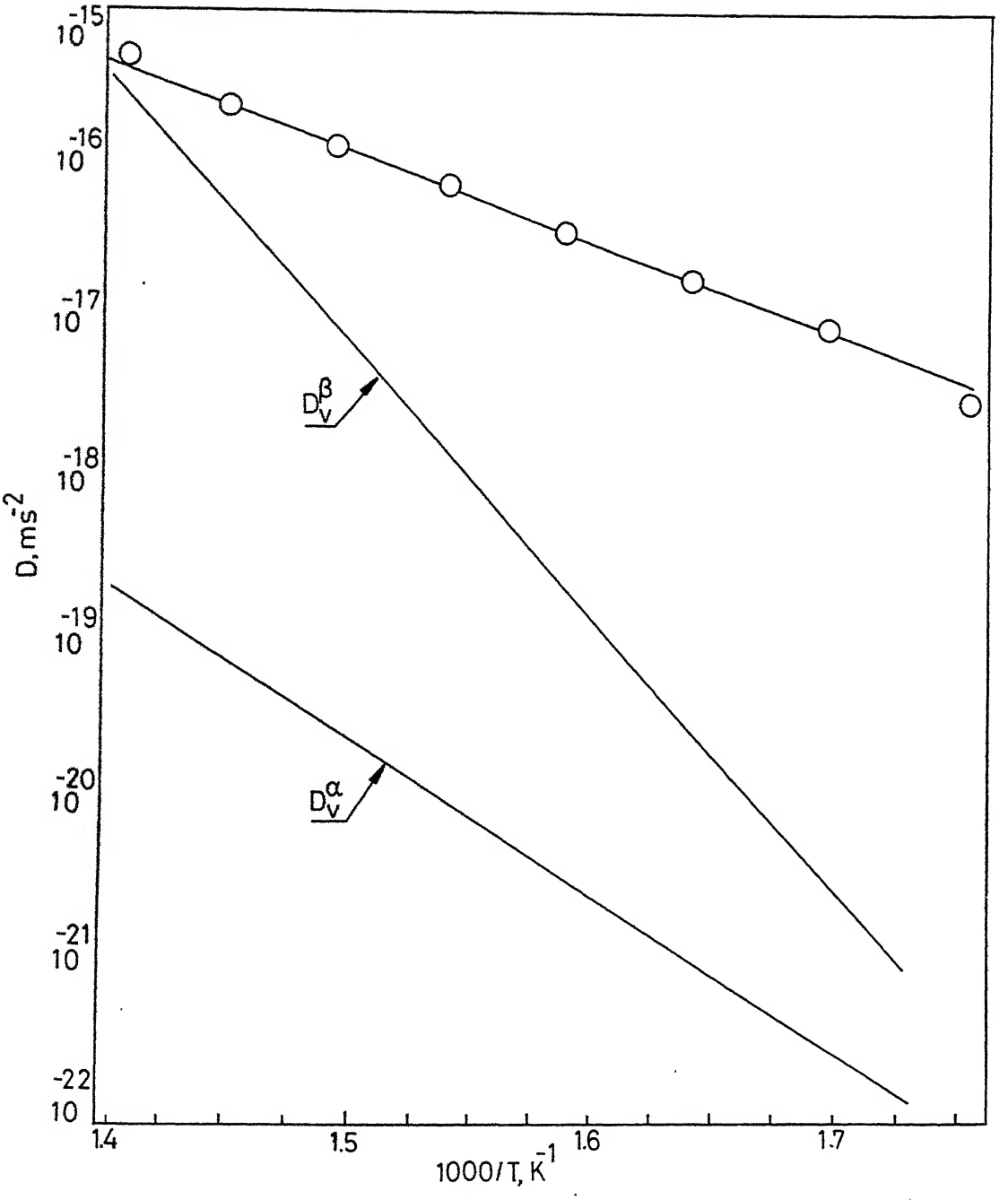

Fig. 19. Semilog plot of D vs. $\frac{1}{T}$, temperature dependence of D_v^{α} and D_v^{β} are also shown.

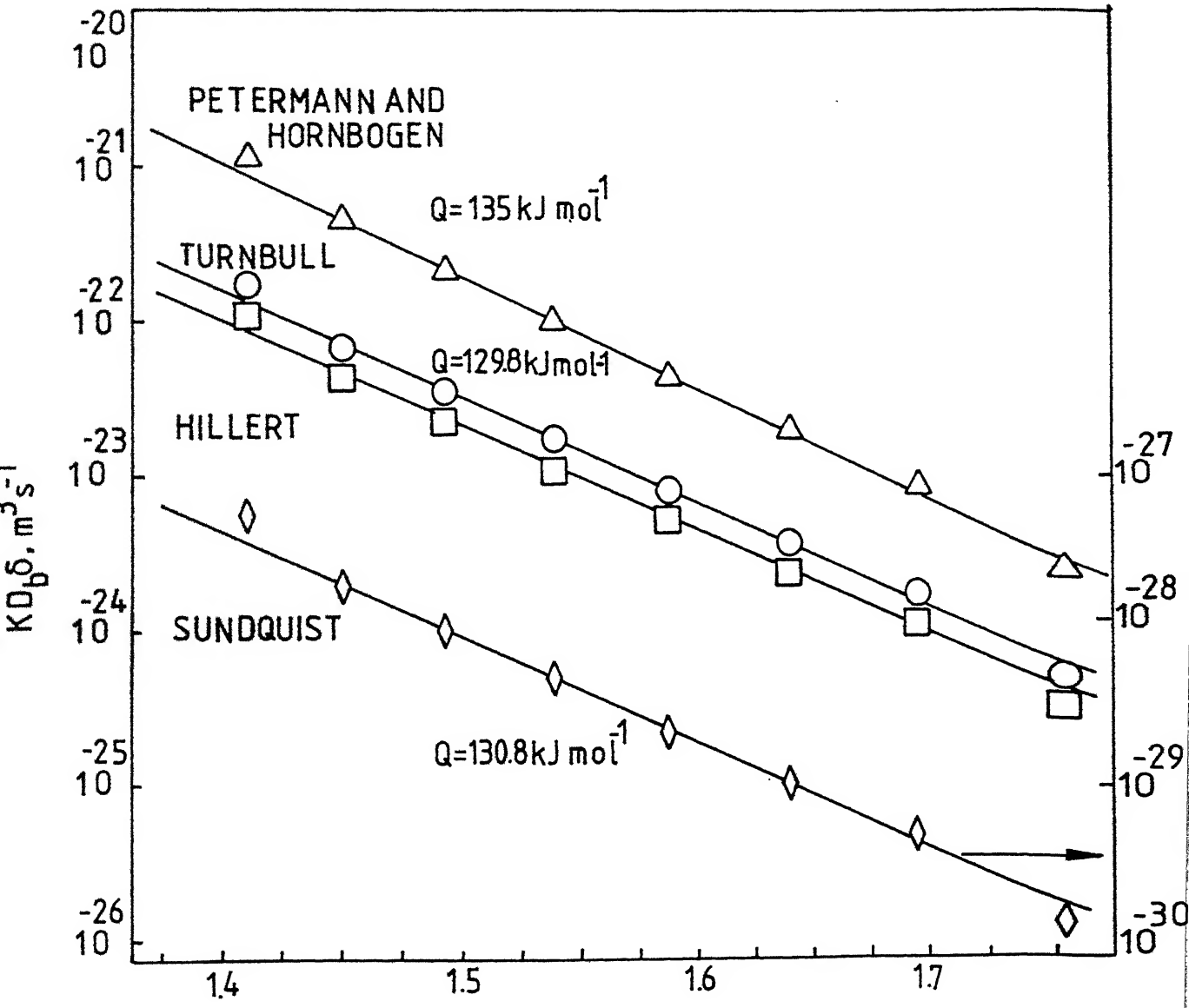

Fig. 20. $KD_b\delta$ vs. 1/T.

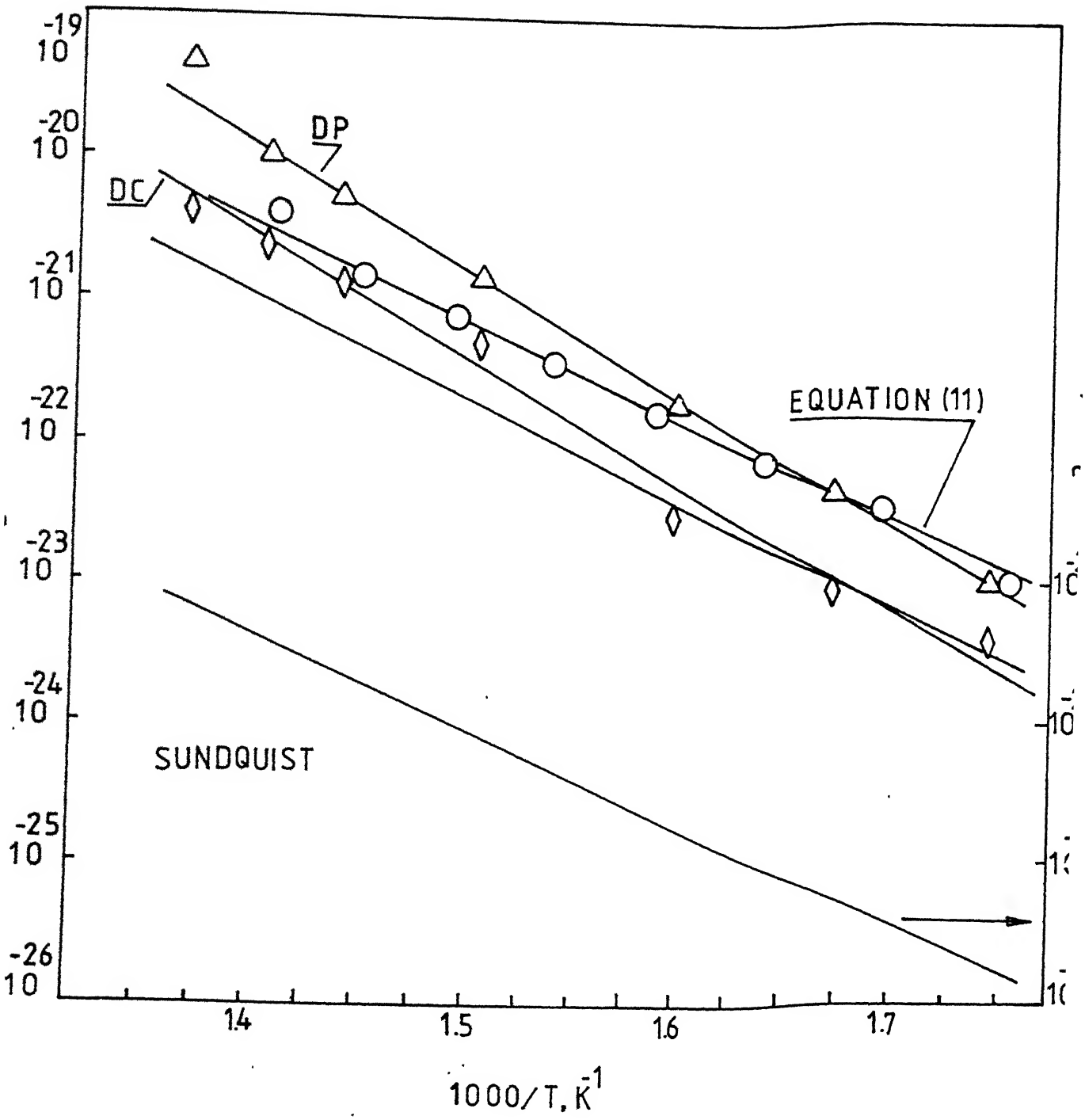

Fig. 21. $KD_b\delta$ vs. 1/T, the diffusivity values obtained during discontinuous precipitation and discontinuous coarsening are also shown for comparison.

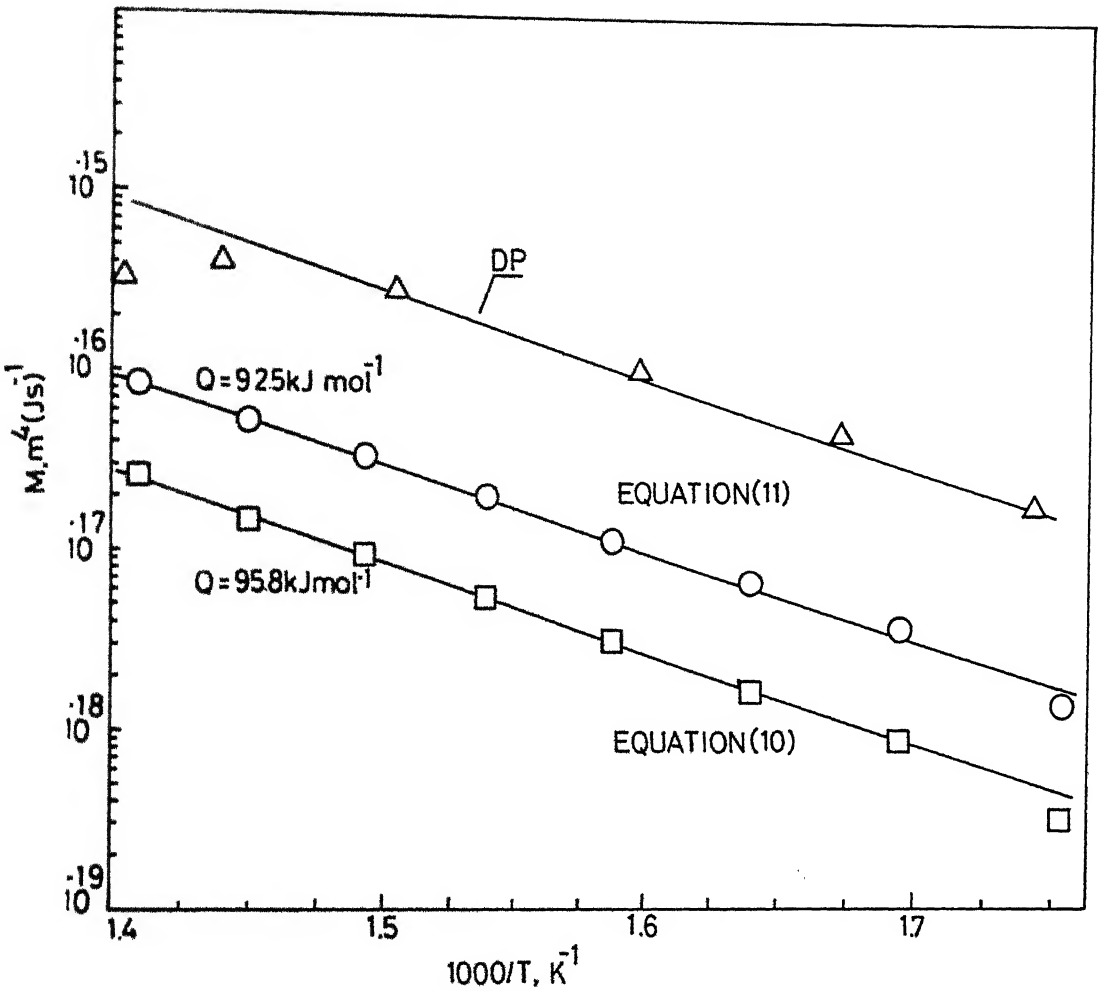

Fig. 12. Mobility vs. 1/T, the mobility obtained during discontinuous precipitation is also shown for comparison.

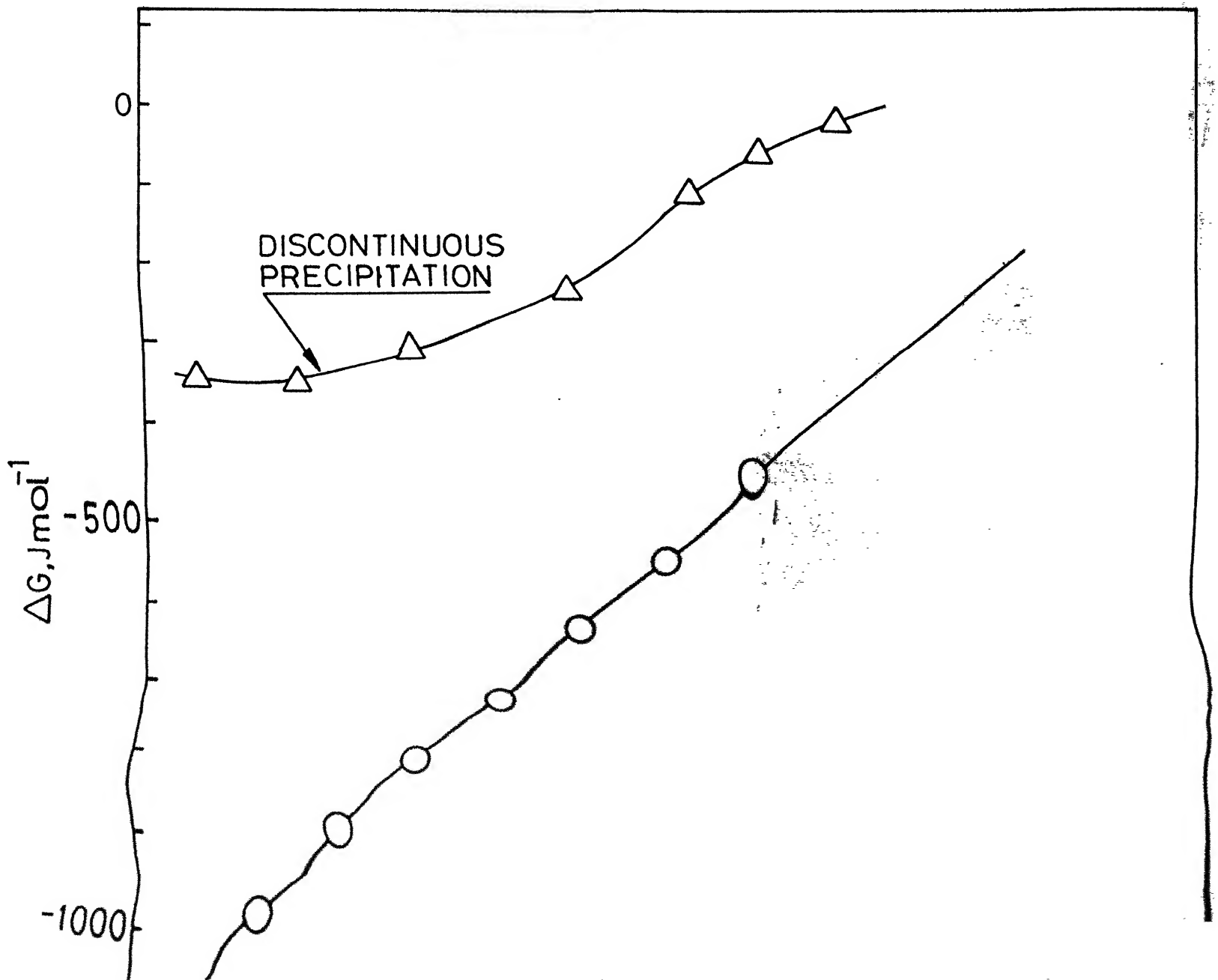
0
-500
-1000
ΔG, Jmol⁻¹
DISCONTINUOUS
PRECIPITATION